



Numerical Strategies for Partitioned Fluid-Structure Interaction Algorithms

Mathieu Olivier and Guy Dumas

*Laboratoire de Mécanique des Fluides Numérique, Département de Génie Mécanique,
Université Laval, Québec, G1V 0A6, Canada*

Email: mathieu.olivier.2@ulaval.ca

ABSTRACT

Two partitioned fluid-structure interaction schemes are presented and compared in this paper which is concerned with aeroelasticity involving large-displacements deforming bodies. The first scheme is implicit while the second is explicit. It is shown how artificial and physical compressibility can be used to stabilize such schemes that are known to be unstable otherwise. Simulations involving flexible flapping plates that can be used as propulsion devices are also presented.

1 INTRODUCTION

In the last several years, the interest in numerical solutions of fluid-structure interaction (FSI) problems has increased significantly in many fields of research such as aeronautics, biology, civil engineering, etc. In that context, many developments have been made to solve such class of problems. These developments are justified by the fact that, although efficient numerical methods exist for both fluid and solid mechanics problems, the solution of fully coupled aeroelastic problems is generally not a straightforward task.

Existing FSI coupling method involving large-displacement elastic solids and incompressible flows can be split into two categories: *partitioned* and *monolithic* (sometimes refer to as *direct*). The idea behind partitioned methods is to use state-of-the-art software and thus benefit from existing optimized technologies in both fluid and solid mechanics. This paradigm assumes that the coupling between both solvers is relatively cheap in terms of computational resources and stable. On the opposite, the objective of monolithic methods is to develop a robust global numerical tool that can handle FSI problems. In that approach, it is assumed that the method may outperform the previous

one in terms of stability and performance (particularly in the case of strong interactions), and that the cost of more robust and more complex algorithms is worth the increase in overall performance.

While it is often mentioned that partitioned solver are good for weak FSI whereas monolithic solvers are well suited for strong FSI, comparing rigorously monolithic and partitioned solvers is not an easy task because there exists a wide variety of schemes in both methodologies. Heil et al. [4] compared the partitioned and the monolithic coupling schemes within the same finite-element framework. In that context, they found that for a finite number of tested problems, the monolithic method outperform the partitioned method where the fluid-solid interaction is strong (in the case of very strong interactions, the latter is even reported to be non-convergent). In the case of weak interaction, both method appear to be equivalent. In that context, the monolithic method seems to be the best coupling method. However, completely monolithic method are known to produce large and complex linear system that are often very expensive in terms of computational resources which justifies the quest to develop convergent and efficient partitioned algorithms.

The reason why the partitioned method is sometimes inefficient or even unstable is now well known and sometimes refer to as the added-mass effect. The problem lies in the incompressibility constraint of the fluid as reported by Causin et al. [1] who also present some interesting analysis using a simplified FSI model. Firstly, an explicit partitioned scheme is unconditionally unstable when the strength of the interaction reaches some level. Secondly, for the implicit partitioned scheme to be stable, a relaxation coefficient must be used between each outer-iteration. It is further shown that the relaxation factor must be smaller for strong interactions and small time-steps,

which may impair significantly the convergence rate of the method. Fortunately, some authors provide alternatives that allow to increase the efficiency and/or stabilize partitioned methods. Among these methods, the artificial compressibility approach [3, 5] appears to be efficient and simple.

In this paper, we present two partitioned FSI coupling schemes that are intended to model strong fluid-solid interactions involving large structural displacements. The first one is an implicit scheme based on a fixed-point iterative procedure. The artificial compressibility method is used to stabilize the scheme when needed. Therefore, this scheme is similar to the one presented by Degroote et al. [3]. The second one is an explicit scheme. It is shown that using a slightly compressible flow model allows to stabilize such a scheme. A brief description of the mathematical models and numerical discretization methods used is presented first. Then, the FSI coupling strategies are presented. At last, some numerical experiments that establish the potential of the proposed schemes are presented. An important contribution of this work is thus to show how to obtain an efficient coupling scheme by using a judicious combination of physical and artificial compressibility.

2 MATHEMATICAL MODELS

In this paper, we deal with the following models: incompressible and slightly compressible flows as well as elastic solids and beam structures involving large displacements. All these continuous media obey the following conservation laws (in an arbitrary moving control volume formulation), namely the space conservation, the mass conservation, and the momentum conservation:

$$\frac{\partial}{\partial t} \int_{V(t)} dV - \int_{S(t)} \hat{\mathbf{v}} \cdot \hat{\mathbf{n}} dS = 0, \quad (1)$$

$$\frac{\partial}{\partial t} \int_{V(t)} \rho dV + \int_{S(t)} \rho \mathbf{c} \cdot \hat{\mathbf{n}} dS = 0, \quad (2)$$

$$\frac{\partial}{\partial t} \int_{V(t)} \rho \mathbf{v} dV + \int_{S(t)} \rho \mathbf{v} (\mathbf{c} \cdot \hat{\mathbf{n}}) dS = \int_{V(t)} \mathbf{f} dV + \int_{S(t)} \hat{\mathbf{n}} \cdot \boldsymbol{\sigma} dS, \quad (3)$$

where ρ is the density field, \mathbf{v} is the velocity field, $\hat{\mathbf{v}}$ is the control surface velocity, $\mathbf{c} = \mathbf{v} - \hat{\mathbf{v}}$, \mathbf{f} is a body force, and $\boldsymbol{\sigma}$ is the stress field. Note that Eq. (1), does

not bring information on any physically meaningful field, but must nonetheless be respected in the numerical implementation in order to avoid spurious mass generation. Slightly compressible barotropic Newtonian flows are governed by the following constitutive laws:

$$\boldsymbol{\sigma} = -p\mathbf{I} + \mu(\nabla\mathbf{v} + \nabla\mathbf{v}^T), \quad (4)$$

$$\rho = \rho_{\text{ref}} + \Psi(p - p_{\text{ref}}), \quad (5)$$

where p is the pressure field, μ is the dynamic viscosity, and Ψ is the compressibility coefficient of the fluid. Of course, in the case of incompressible flows, $\Psi = 0$.

Elastic structures involving large displacements are governed by the same conservation laws. A total Lagrangian formulation is used in this work for the solid media, so that the velocity of the control volume is the same as the physical medium itself ($\hat{\mathbf{v}} = \mathbf{v}$ and $\mathbf{c} = \mathbf{0}$). Furthermore, the equations are expressed in terms of the initial state. The momentum conservation equation (Eq. (3)) then becomes:

$$\frac{\partial}{\partial t} \int_{V_0} \rho_0 \mathbf{v} dV_0 = \int_{V_0} \mathbf{f}_0 dV_0 + \int_{S_0} \hat{\mathbf{n}} \cdot (\mathbf{S} \cdot \mathbf{F}^T) dS_0, \quad (6)$$

where \mathbf{S} is the second Piola-Kirchhoff stress tensor, $\mathbf{F} = \mathbf{I} + \nabla_0 \mathbf{u}^T$ is the deformation gradient, \mathbf{u} is the displacement field, and the subscript 0 refers to the initial state of the solid medium. The constitutive law of an elastic solid is given by the St. Venant-Kirchhoff law:

$$\mathbf{S} = 2\nu\mathbf{E} + \lambda \text{tr}(\mathbf{E})\mathbf{I}, \quad (7)$$

$$\mathbf{E} = \frac{1}{2}(\nabla_0 \mathbf{u} + \nabla_0 \mathbf{u}^T + \nabla_0 \mathbf{u} \cdot \nabla_0 \mathbf{u}^T), \quad (8)$$

where \mathbf{E} is the Green-Lagrange deformation tensor, and ν and λ are the Lamé coefficients of the structure.

When dealing with thin elongated structures, a nonlinear beam model is also used. This model assumes a linear elastic behaviour but allows large displacements. In that sense, it is equivalent to Eqs. (6) to (8). The Euler-Bernoulli hypotheses are used to obtain a thin-geometry approximation. The governing equations for beam structures defined on the x -axis in a total Lagrangian formulation are, in 2D:

$$\begin{aligned} \rho A \frac{\partial^2 u_x}{\partial t^2} &= \frac{\partial}{\partial x} \left[N \left(1 + \frac{\partial u_x}{\partial x} \right) \right] \\ &+ \frac{\partial}{\partial x} \left[M \frac{\partial^2 u_y}{\partial x^2} \right] + \frac{\partial^2}{\partial x^2} \left[M \frac{\partial u_y}{\partial x} \right] \\ &+ f_x - \tilde{p} \frac{\partial u_y}{\partial x} + \tilde{\tau} \left(1 + \frac{\partial u_x}{\partial x} \right), \quad (9) \end{aligned}$$

$$\begin{aligned} \rho A \frac{\partial^2 u_y}{\partial t^2} &= \frac{\partial}{\partial x} \left[N \frac{\partial u_y}{\partial x} \right] \\ &- \frac{\partial^2}{\partial x^2} \left[M \left(1 + \frac{\partial u_x}{\partial x} \right) \right] - \frac{\partial}{\partial x} \left[M \frac{\partial^2 u_x}{\partial x^2} \right] \\ &+ f_y - \tilde{p} \left(1 + \frac{\partial u_x}{\partial x} \right) - \tilde{\tau} \frac{\partial u_y}{\partial x}, \end{aligned} \quad (10)$$

where \tilde{p} is the lineic pressure, $\tilde{\tau}$ is the lineic shear stress, both acting on the deformed configuration. The normal stress N and the bending moment M are given by:

$$N = EA \left[\frac{\partial u_x}{\partial x} + \frac{1}{2} \left(\left(\frac{\partial u_x}{\partial x} \right)^2 + \left(\frac{\partial u_y}{\partial x} \right)^2 \right) \right], \quad (11)$$

$$M = EI \left[\frac{\partial^2 u_y}{\partial x^2} \left(1 + \frac{\partial u_x}{\partial x} \right) - \frac{\partial u_y}{\partial x} \frac{\partial^2 u_x}{\partial x^2} \right], \quad (12)$$

where E is the Young modulus, A and I are respectively the area and the inertia of the beam section.

3 NUMERICAL DISCRETIZATION

Since the objective of the paper is to establish guidelines for the choice of FSI partitioned coupling schemes, three fluid flow solvers and two structural solvers are considered.

3.1 Fluid Flow Solvers

The first fluid flow solver involves incompressible flows. It is an implicit solver that uses the segregated second-order finite volume method. The pressure is treated with a Poisson equation in a SIMPLE or PISO manner. Time integration is performed with the backward scheme which is also second-order accurate. This solver has been discussed in further details in a previous conference [6].

The second flow solver is very similar to the last one, but it uses the barotropic model (Eq. (5)). The major difference thus lies in the discretized pressure equation where some additional terms takes the compressibility into account. Otherwise, the algorithms and schemes are the same.

The third flow solver is fully explicit. It is also based on the barotropic equation of state (Eq. (5)). Therefore, to obtain an incompressible flow solution, the compressibility coefficient ψ must be chosen so that the Mach number $Ma = V_{\text{ref}} \sqrt{\psi}$ is sufficiently small (recall that the speed of sound $c = \sqrt{\frac{\partial p}{\partial \rho}} = \sqrt{\frac{1}{\psi}}$). The choice of using a slightly compressible flow solver

rather than an incompressible one for the explicit scheme is justified as follow:

- The resulting algorithm is matrix-free whereas an explicit algorithm for incompressible flow involves the solution of an elliptic problem for the pressure which generates a linear system.
- Ultimately it will be shown that the added-mass instability is removed (as expected) when using a compressible fluid.

Of course, such a strategy has the drawback that an additional time-step size restriction stability condition is necessary in the fluid solver (the third constraint below):

$$\frac{\|\mathbf{v}\| \Delta t}{\Delta x} < O(1); \quad \frac{\nu \Delta t}{\Delta x^2} < O(1); \quad \frac{\Delta t}{\sqrt{\psi} \Delta x} < O(1); \quad (13)$$

where ν is the kinematic viscosity. Here again, the second order finite volume method is used for the spatial discretization whereas the first order Euler integration scheme is used for temporal discretization. The choice of a first order integration scheme is justified by two factors. First, it is more economical and, second, since the time-step is very small as it is related to the stability constraint in the solid solver (see section 3.2), the first order precision is most likely to be sufficient.

All these solvers are implemented with moving mesh support, that is, Eq. (1) is taken into account. The mesh motion is smoothed over the domain based on partial differential equations (such as the Laplace or the pseudo-solid equation) or on radial extrapolation techniques.

3.2 Structural Solvers

The first structural solver is based on the general solid model (Eqs. (6) to (8)). The implementation is also done with the segregated finite volume method. Since the method is segregated, the implicit algorithm involves explicit terms that are made implicit through an iterative process (inter-component coupling and non-linear terms). A Newton-Raphson linearization is thus not possible. However the resulting matrices are less complex and diagonally dominant. This has the consequence that for relatively small time-steps, the performance of the method is excellent. On the other hand, when large time-step or steady-state situations occur, the convergence rate deteriorates (see [6] for further details). Alternatively, the solver can be configured to use the explicit central difference method to perform

the time integration. In that context, a typically severe stability condition appears:

$$\frac{\Delta t}{\Delta x} \sqrt{\frac{E}{\rho}} < O(1), \quad (14)$$

which is similar to the third condition in Eq. (13) as they are both a CFL-type condition based on the speed of sound in their respective media. The second structural solver is based on the beam model (Eqs. (9) to (12)). The Galerkin finite element method is used in conjunction with Hermite shape functions. The Newton-Raphson method is used to linearize the problem. The time integration is performed with a second order backward scheme. This solver can also be configured to use the explicit central difference method to perform the time integration.

4 FLUID-SOLID COUPLING STRATEGIES

4.1 Implicit Coupling Using Artificial Compressibility

The implicit coupling algorithm is built with the incompressible flow solver in mind, although it can also be used with the barotropic solver. An artificial compressibility source term is added in the pressure equation to stabilize the coupling. This term has the form:

$$\int_{V(t)} \frac{\tilde{\Psi}}{\Delta t} (p_{i+1}^{n+1} - p_i^{n+1}) dV, \quad (15)$$

where $\tilde{\Psi}$ is the artificial compressibility, i is the outer-iteration counter and n is the time-step counter. Therefore, at the end of a time-step, this term tends toward zero (up to a specified tolerance) hence providing an incompressible flow solution when the incompressible flow solver is used. When the barotropic solver is used instead, the remaining compressibility at the end of the iterative process is strictly physical. The artificial compressibility assumes a non-zero value only in the first cell layer next to the FSI interface and zero elsewhere, following Degroote et al. [3]. Here, the artificial compressibility $\tilde{\Psi}$ is set as a constant as small as possible to obtain a good convergence rate without compromising the stability. The overall algorithm corresponds to the following steps:

1. Beginning of time-step.
2. Solution of the solid displacement field using the fluid stress field from the previous time-step as a Neumann boundary condition. This gives a displacement predictor.

3. Computation of the new mesh points using the displacement predictor.
4. Solution of the fluid fields (velocity and pressure) using the displacement predictor as a Dirichlet boundary condition.
5. Outer loop:
 - Solution of the solid displacement field. Partial convergence is sufficient as long as it does not impair the convergence rate.
 - Actualization of the interface position. The rest of the mesh remains fixed.
 - Solution of the fluid velocity and pressure fields. The artificial compressibility term given by Eq. (15) is used in the continuity equation to stabilize the coupling. Again, partial convergence is sufficient as long as it does not impair the convergence rate.
 - Check convergence of residuals of all quantities (solid displacement, fluid velocity and pressure).
6. End of time-step.

4.2 Explicit Coupling for Slightly Compressible Barotropic Flow

The second FSI scheme that is presented is explicit. Such a scheme is prone to be unconditionally unstable when the fluid-solid interaction is too strong. To remove this unstable character, it is proposed in this work to use the barotropic explicit flow solver with a small physical compressibility coefficient. Such a formulation removes the elliptic character of the pressure equation and, at the same time, the added-mass instability. The resulting FSI scheme is fairly simple and is given by these steps:

1. Beginning of time-step.
2. Solution of the solid displacement field using an explicit scheme. The fluid stress from the previous time-step is used as a Neumann boundary condition, which is consistent with the explicit scheme.
3. Computation of the new mesh points using the previously computed displacement field.
4. Solution of the fluid field using the new mesh and the interface velocity as a Dirichlet boundary condition.

5. End of time-step.

Obviously, such a scheme needs to respect all stability conditions to remain stable (Eqs. (13) and (14)).

4.3 Interface Treatment

The FSI interface conditions are treated as follow: the solid velocity is applied in the fluid solver as a Dirichlet boundary condition and the fluid load (pressure and viscous) is applied in the solid solver as a Neumann boundary condition. In order to allow the use of non-matching meshes at the interface, a Radial-Basis-Function (RBF) interpolation is used, following the recommendations of de Boer et al. [2]. The radial function used in the RBF interpolation is a thin-plate spline ($r^2 \log(r)$).

5 NUMERICAL EXPERIMENTS AND RESULTS

In this section, the case of a 2D flexible flapping plate is studied and tested with different coupling strategies. The geometry is taken as a 2%-thick flat plate of chord c with rounded edges which has a heaving motion imposed on the leading edge (LE):

$$y_{LE} = h \cos(2\pi ft). \quad (16)$$

The dimensionless parameters of the whole aeroelastic problem are thus:

$$Re = \frac{\rho_f U_\infty c}{\mu} = 800, \quad Re_f = \frac{\rho_f h f c}{\mu} = 200, \quad \frac{h}{c} = 1, \\ E^* = \frac{E}{\rho_f h^2 f^2} = 6.24 \times 10^7, \quad D^* = \frac{\rho_s}{\rho_f} = 6.25.$$

The compressibility coefficient of the fluid is set to obtain a nearly incompressible flow ($Ma < 0.01$) in the case of simulations involving the barotropic model. These parameters provide a case where the fluid-solid interaction is strong. This problem is thus a good candidate to evaluate the potential of each proposed FSI scheme.

The mesh of the fluid domain consists of a 58604-cells elliptically smoothed quadrilateral O-grid mesh. This mesh has proven to be sufficient for this specific case since the oscillating frequency is relatively slow and the wake of the wing is rapidly convected downstream so that there is no significant wing-wake interaction. The mesh of the solid domain is made of a 10×100 quadrilateral cells distribution in the case of the finite-volume solver. Simulations using the beam model are

done with a 50 beam-elements mesh. Initial conditions consist of a uniform flow within the whole domain. Therefore, this situation represents an impulsively started flow. The flow velocity U_∞ is imposed on the left side of the circular domain while an out-flow condition is imposed on the other side. Table 1 presents a summary of the solver combinations that have been tested using different FSI schemes.

In these simulations, residual tolerances were the same for all simulations in order to illustrate the effect of refining the time-step on the number of outer-iterations. These tolerances have proven to be sufficiently small for all cases except case E, for which the simulation was also run with residual tolerance one order of magnitude smaller (results in parenthesis in table Table 1).

It is observed that, even though simulations with a smaller time-step converge, the convergence rate deteriorates to such a point that the maximum number of iterations is reached before convergence is achieved when the incompressible flow solver is used (case B and C). This behavior is contrary to what is expected and sought for when using a segregated approach. Indeed, it would be desirable that reducing the time-step (without changing the residual tolerance) reduces the required number of iterations since the initial guess provided by the previous time-step is better. However, it is also observed that not only the pressure field is always the last one to reach its convergence criterion, it also converges more slowly than all other quantities.

It can be concluded that those simulations still have some significant residual in the pressure equation coming from the artificial compressibility term (Eq. (15)). However, results of simulations B and C are found to be in very good agreement with other simulations even though their pressure fields did not reach the desired tolerance (see, for instance, Fig. 1), which tends to support the assumption that the remaining residual of the artificial compressibility term is not physically significant even if the pressure equation residual is still relatively high compared to other equations. Short of a systematic verification, it is thus not possible yet to determine if this remaining compressibility is significant or not without comparing the actual results with a reference solution.

That is where the use of a barotropic model becomes interesting. Indeed, using this model, it is possible to set what would appear to be an additional compressibility from the algorithmic point of view. This compressibility acts as if it was the residual noise of the artificial compressibility term except that it has a physical meaning and that it can be quantified. This strategy is found to be successful.

Table 1: Simulations using different FSI schemes and solver combinations.

ID	Solid solver	Fluid solver	$f\Delta t$	$\tilde{\psi}h^2f^2$	Average number of outer-iterations	$(u_{y,TE} - u_{y,LE})/c$ $ft = 0.04$	$(u_{y,TE} - u_{y,LE})/c$ $ft = 0.125$
A	Beam	Incompressible	0.0005	0.0075	6.7	0.047197	0.15278
B	Beam	Incompressible	0.0001	0.00025	40*	0.047222	0.15279
C	StVK	Incompressible	0.0001	0.0125	40*	0.046787	0.14944
D	Beam	Barotropic	0.0005	0.0025	5.4	0.047205	0.15279
E**	Beam	Barotropic	0.0001	0	2.7 (7.1)	(0.047221)	(0.15280)
F	StVK	Barotropic	0.0001	0	7.7	0.046816	0.15429
G	StVK-expl.	Barotropic-expl.	5×10^{-9}	-	-	0.046767	-

* Maximum number of iterations reached before convergence criteria is met.

** Number in parenthesis correspond to the solution using a finer residual tolerance.

Indeed, as reported in Table 1, simulations involving the barotropic model always converge in less iterations than their incompressible counterparts. Furthermore, simulations with a smaller time-step need less iterations to reach the same convergence tolerance, which is a desirable property that is not achieved when the incompressible flow solver is used. Also, these simulations with a smaller time-step do not require artificial compressibility at all. This is explained by the fact that the elliptic character of the pressure equation is lost when the barotropic model is used.

In terms of required CPU time, Table 2 shows the relative cost of the complete FSI simulation with respect to each single-field simulation. The first column corresponds to the first few time-steps of the simulation while the second column corresponds to the rest of the simulation. The reason for that distinction is to discriminate the effect associated to the impulsive start-up which usually increases the number of outer-iterations.

Each single-field simulation is performed with the same solver parameters except for these modifications: the FSI interface is moved according to the imposed

motion of the leading edge in the fluid simulation and a constant traction boundary condition is imposed on the FSI interface in the solid simulation. Furthermore, the fluid simulation is carried-out without artificial compressibility. The overall result is that the overhead associated to the FSI coupling is very small.

Regarding the explicit FSI scheme, as stated earlier, only the barotropic fluid solver can provide a stable scheme. Furthermore, the beam solver appears to be unstable, even when the time-step respects all stability conditions. This is probably attributed to the fact that the data exchange at the FSI interface is not energy-conservative. Indeed, while the pressure and shear forces are treated as uniform per element in the current beam formulation, the displacement is supported by cubic polynomials which is not consistent with the finite-volume formulation.

On the other hand, the explicit simulation using the finite-volume structural solver is convergent but the required time-step to provide stability is about 10^5 times smaller than implicit simulations (see case G in Table 1). This is explained by the fact that the stability constraint within the solid is closely related to the velocity of sound which is very high when compared to the characteristic velocities involved in the flow field. Therefore, even though this explicit FSI scheme is completely matrix-free, the overhead associated to the very small time-step is too much restrictive for that method to be efficient when dealing with hardly compressible solids.

Of course, differences in the numerical results between

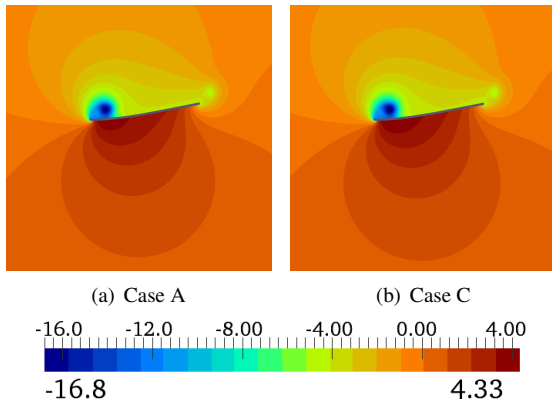


Figure 1: Pressure coefficient at $ft = 0.125$.

Table 2: Relative simulation times for case D

	$ft < 0.125$	$ft > 0.125$
T_S	0.00353	0.00659
T_F	0.645	0.839
T_{FSI}	1	1
$T_{FSI}/(T_S + T_F)$	1.54	1.18

each simulation are to be expected since different models are used. However, these differences remain small since the differences between each model is subtle (see last two columns of Table 1 as well as Fig. 3 and Fig. 4). Because the barotropic model allows pressure waves to develop, it is instructive to look at the pressure coefficient fields of the simulations which are defined as:

$$C_p = \frac{p - p_\infty}{\frac{1}{2}\rho_f U_\infty^2}. \quad (17)$$

Indeed, a pressure wave associated to the initial impulsion is present in simulations using this model (Fig. 2). However, as expected, this pressure wave dissipates with time since it is closely related to the impulsive start-up. Indeed, Fig. 3 shows that no pressure waves are present after the initial few time-steps and that the pressure field is not significantly affected by the use of a barotropic model since Ma is small.

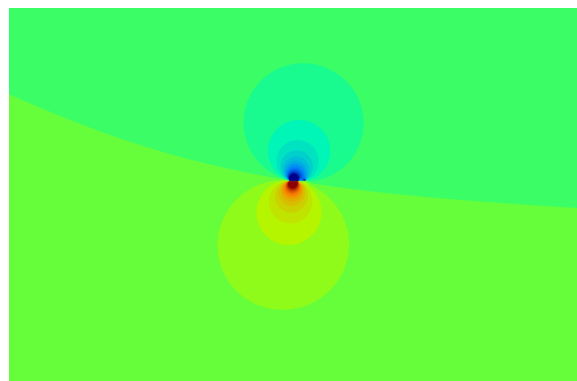
Moreover, the calculation of force coefficients remains unaffected as it is shown in Fig. 4. Secondly, the time-step size still has a repercussion on simulations exhibiting a pressure wave since the time-step is not small enough to capture this wave accurately (the time-step size is adjusted to the flow velocity). However, this is not a concern here since we try to mimic incompressible flows. Indeed, Fig. 2 shows that when the pressure wave is damped out by a larger time-step, the pressure field approaches its incompressible counterpart.

Lastly, the difference in results between the beam model and the general solid model appears to be negligible for practical purposes (see Table 1). However, the beam model proved to be numerically much more efficient. This can be explained by two reasons:

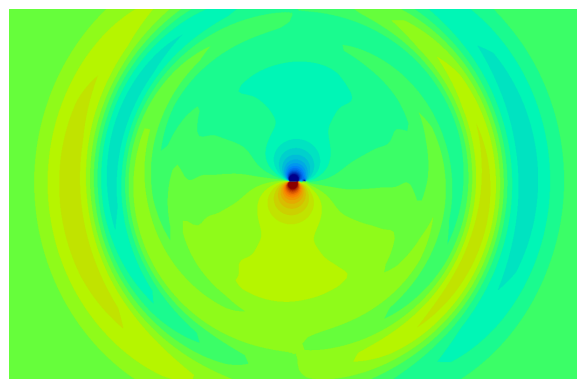
- the beam model contains less degrees of freedom (obviously);
- the beam model uses a Newton-Raphson linearization.

The segregated finite-volume solid solver would be an appropriate choice for cases where the time scale associated to velocity of sound is close to the characteristic time scales of the flow, which is rarely the case. Otherwise, a fully coupled structural solver with possibly a Newton-Raphson linearization would be more appropriate for general 3D geometries.

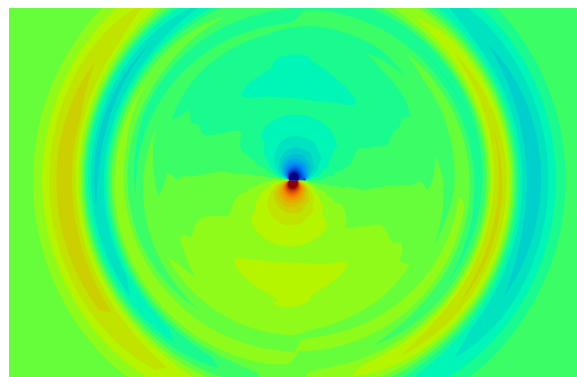
As it was stated earlier, this oscillating flapping plate problem represents a propulsion device involving strong fluid-solid interaction. The thrust coefficient is



(a) Case A



(b) Case D



(c) Case E

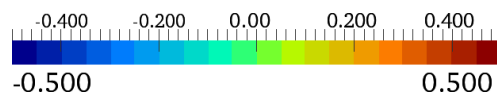
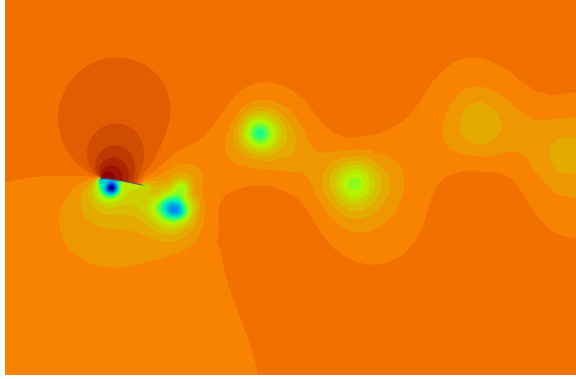


Figure 2: Far-field pressure coefficient near the beginning of the simulation ($ft = 0.025$).

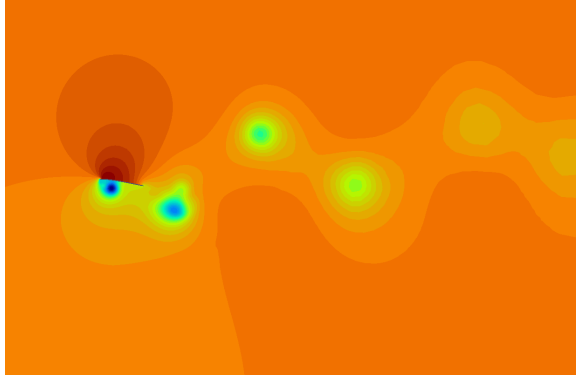
defined by:

$$C_{T,LE} = -\frac{F_x}{\frac{1}{2}\rho_f U_\infty^2 c},$$

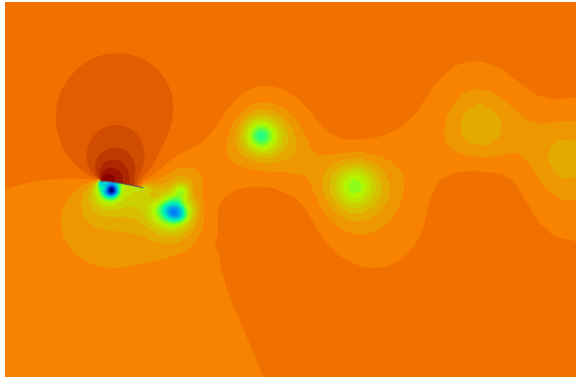
where F_x is the x component of the force per unit depth on the driving mechanism located on the leading edge. Therefore, that force is the structural reaction on the



(a) Case A



(b) Case D



(c) Case E

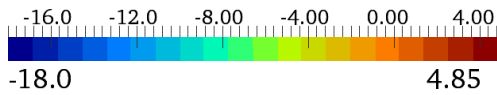


Figure 3: Pressure coefficient a long time after the start-up ($ft = 5.75$).

driving mechanism, which includes a component associated to the inertia of the plate and a component associated to external aerodynamic forces. In order to establish a comparison, the aerodynamic thrust coefficient can be obtained by using the same definition while replacing the structural reaction with the aerodynamic force on the FSI interface. As it is shown

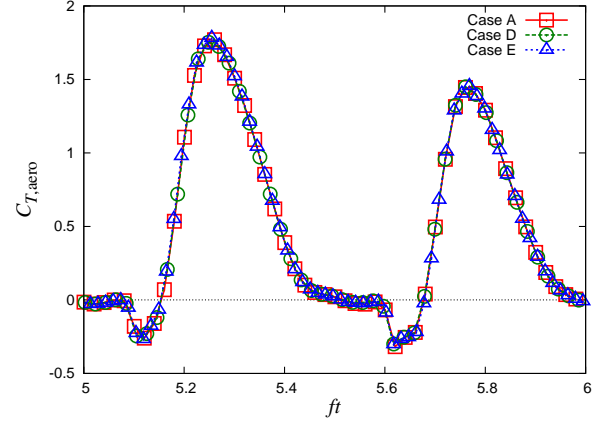


Figure 4: Aerodynamic thrust coefficient of the whole plate for the last simulation cycle using different models and parameters.

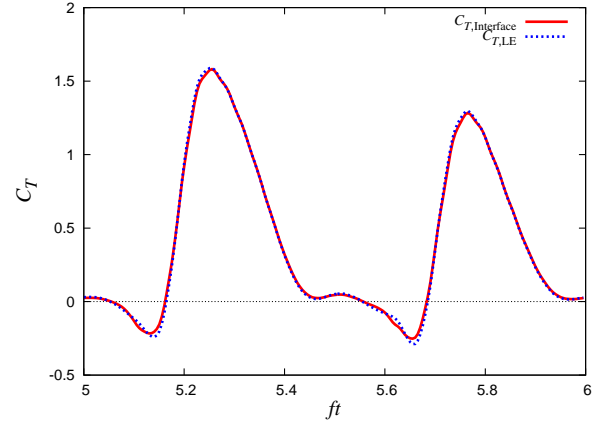


Figure 5: Comparison between the structural reaction on the LE and the aerodynamic force on the FSI interface.

on Fig. 5, the aerodynamic thrust coefficient on the FSI interface is almost the same as the structural thrust coefficient on the leading edge. Furthermore, Fig. 6 shows that the plate deflection is closely related to the pressure field. That confirms that the fluid-solid interaction is strong and that the plate inertia plays a secondary role. Lastly, it is interesting to observe how the plate deflection acts as a passive pitching angle that helps to orient the aerodynamic force in the direction of the flow, thus improving the thrust of the plate (see Fig. 5 and Fig. 6 at $ft = 5.250$ and $ft = 5.750$).

6 CONCLUSION

This paper shows that an artificial compressibility source term in the pressure equation allows to stabilize efficiently an implicit partitioned FSI scheme. Furthermore, the use of physical compressibility through the barotropic model allows to control the residual

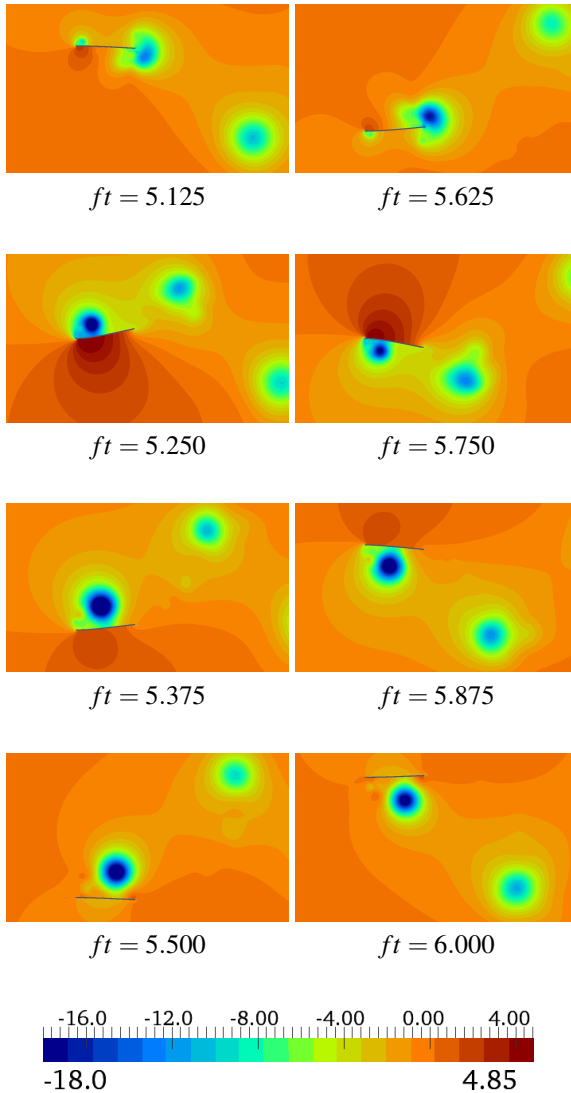


Figure 6: Evolution of the pressure coefficient field.

of the artificial compressibility source term when the convergence is harder to achieve. Moreover, the barotropic model allows to build a completely explicit FSI scheme.

Numerical experiments on the case of a flexible oscillating plate in propulsion regime involving strong fluid-solid interaction are presented. It is shown that the overhead of the implicit FSI procedure is very small when compared to single field simulation times, thus allowing to benefit from state-of-the-art optimized technologies in both media. It is also demonstrated that the barotropic model can be used efficiently to model nearly incompressible flows. On the other hand, the explicit scheme suffers from very restrictive stability conditions.

ACKNOWLEDGEMENTS

The authors acknowledge financial support from FQRNT Québec and NSERC Canada as well as high-performance computing infrastructures provided by CLUMEQ and Compute Canada.

REFERENCES

- [1] P. Causin, J.F. Gerbeau, and F. Nobile. Added-mass effect in the design of partitioned algorithms for fluid-structure problems. *Computer Methods in Applied Mechanics and Engineering*, 194:4506–4527, 2005.
- [2] A. de Boer, A.H. Van Zuijlen, and H. Bijl. Review of coupling methods for non-matching meshes. *Computational Methods in Applied Mechanics and Engineering*, 196:1515–1525, 2007.
- [3] J. Degroote, A. Swillens, P. Bruggement, R. Haelterman, P. Segers, and J. Vierendeels. Simulation of fluid-structure interaction with the interface artificial compressibility method. *International Journal for Numerical Methods in Biomedical Engineering*, 26:276–289, 2010.
- [4] M. Heil, A.L. Hazel, and J Boyle. Solvers for large-displacement fluid-structure interaction problems : Segregated versus monolithic approaches. *Computational Mechanics*, 43:91–101, 2008.
- [5] E. Järvinen, P. Råback, M. Lyly, and J.P. Salenius. A method for partitioned fluid-structure interaction computation of flow in arteries. *Medical Engineering and Physics*, 30:917–923, 2008.
- [6] M. Olivier and G. Dumas. Non-linear aeroelasticity using an implicit partitioned finite volume solver. Ottawa, Canada, May 2009. 17th Annual Conference of CFD Canadian Society, Paper CFD-2009-5B1.